

The relationship between star formation rate and radio synchrotron luminosity at $0 < z < 2$

Timothy Garn^{1*}, David A. Green², Julia M. Riley², Paul Alexander^{2,3}

¹*SUPA, Institute for Astronomy, Royal Observatory Edinburgh, Blackford Hill, Edinburgh EH9 3HJ*

²*Astrophysics Group, Cavendish Laboratory, 19 J. J. Thomson Ave., Cambridge CB3 0HE*

³*Kavli Institute of Cosmology Cambridge, Madingley Road, Cambridge, CB3 0HA*

24 October 2018

ABSTRACT

We probe the relationship between star formation rate (SFR) and radio synchrotron luminosity in galaxies at $0 < z < 2$ within the northern *Spitzer* Wide-area Infrared Extragalactic survey (SWIRE) fields, in order to investigate some of the assumptions that go into calculating the star formation history of the Universe from deep radio observations. We present new 610-MHz Giant Metrewave Radio Telescope (GMRT) observations of the European Large-Area *ISO* Survey (ELAIS)-N2 field, and using this data, along with previous GMRT surveys carried out in the ELAIS-N1 and Lockman Hole regions, we construct a sample of galaxies which have redshift and SFR information available from the SWIRE survey. We test whether the local relationship between SFR and radio luminosity is applicable to $z = 2$ galaxies, and look for evolution in this relationship with both redshift and SFR in order to examine whether the physical processes which lead to synchrotron radiation have remained the same since the peak of star formation in the Universe. We find that the local calibration between radio luminosity and star formation can be successfully applied to radio-selected high-redshift, high-SFR galaxies, although we identify a small number of sources where this may not be the case; these sources show evidence for inaccurate estimations of their SFR, but there may also be some contribution from physical effects such as the recent onset of starburst activity, or suppression of the radio luminosity within these galaxies.

Key words: radio continuum: galaxies – galaxies: evolution – galaxies: high-redshift

1 INTRODUCTION

In recent years there has been much interest in constraining the star formation history of the Universe (e.g. Lilly et al. 1996; Madau et al. 1996; Mobasher et al. 1999; Haarsma et al. 2000; Hopkins et al. 2003; Hopkins 2004; Hopkins & Beacom 2006; Tresse et al. 2007; Seymour et al. 2008; Smolčić et al. 2009; Magnelli et al. 2009). Estimates of the variation in the co-moving star formation rate density (SFRD) of the Universe with redshift can be made from a number of multi-wavelength tracers, with the most common ones being in the optical and infrared regimes (see Kennicutt 1998, for a review of star formation indicators). These estimates can differ by up to an order of magnitude (e.g. Hopkins et al. 2003), which is in part due to the significant uncertainty in the correction factor that needs to be applied for the effects of interstellar dust grains. These grains absorb short-wavelength ultra-violet (UV) and optical radiation, heat up to temperatures of a few tens to hundreds of kelvin, and re-emit thermally with a modified black-body spectrum that peaks in the infrared, thus having a

significant effect on the optical and infrared spectral energy distribution (SED) of a galaxy.

There have been a few attempts to estimate the SFRD of the Universe from radio observations (e.g. Mobasher et al. 1999; Haarsma et al. 2000; Seymour et al. 2008; Smolčić et al. 2009). These studies have a significant advantage over optical and infrared estimates, in that radio observations are unaffected by the presence of dust grains, and do not require the corrections that are needed at other wavelengths. However, there are a number of disadvantages to radio studies, the principal one being that very deep observations are required in order to reach the regime where star-forming galaxies begin to dominate (around $100 \mu\text{Jy}$ at 1.4 GHz, e.g. Seymour et al. 2008). This disadvantage will be overcome with the next generation of radio telescopes such as the Low Frequency Array (LOFAR) and the Square Kilometre Array (SKA), which are expected to routinely reach observation depths where the radio sky is dominated by star-forming galaxies.

The non-thermal radio emission from star-forming galaxies is much greater than the thermal emission at frequencies below a few GHz, and is predominantly made up of synchrotron radiation, with supernova remnants putting energy into a population of electrons which are accelerated through the galactic magnetic field (see e.g.

* E-mail: tsg@roe.ac.uk

Condon 1992). The details of this process are still a subject for debate, with two principal alternatives; that galaxies are optically thick to cosmic rays and act as ‘calorimeters’ (Völk 1989), or that galaxies are optically thin (Chi & Wolfendale 1990; Helou & Bica 1993), and the cosmic rays can diffuse out of the host galaxy. In the former case, the radio flux from a galaxy will be essentially independent of the magnetic field B (e.g. Thompson et al. 2006), since all of the energy from the cosmic rays will be radiated within the galaxy. In the latter case only some fraction of the total energy will be radiated within the galaxy, and variations in the B -field strength of galaxies over time may show up as a variation in the confinement of cosmic rays, and an evolution in the relationship between star formation rate (SFR) and synchrotron luminosity with redshift. Star-forming galaxies with magnetic field strengths of a few μG have been indirectly detected through Faraday rotation measurements out to $z \sim 2$ (Kronberg et al. 2008; Bernet et al. 2008), but the rate and processes which lead to evolution in B -field strength with time are currently unknown.

Attempts to estimate the SFRD of the Universe from radio observations currently rely upon the untested assumption that local relationships between radio luminosity and SFR (e.g. Condon & Yin 1990; Bell 2003) can be applied successfully at higher redshift, and to sources undergoing much more extreme starbursts than are seen in the local Universe. In this work we test these assumptions, using new radio surveys of the three northern *Spitzer* Wide-area Infrared Extragalactic survey (SWIRE; Lonsdale et al. 2003) fields. SWIRE is a 49 deg^2 study of six regions of sky that have particularly low values of background cirrus emission, using the *Spitzer Space Telescope* (Werner et al. 2004). Observations have been made in seven *Spitzer* wavebands with the Multiband Imaging Array for *Spitzer* (MIPS; Rieke et al. 2004) and the Infrared Array Camera (IRAC; Fazio et al. 2004) between $3.6 \mu\text{m}$ and $160 \mu\text{m}$. The three SWIRE fields studied in this work are in the northern hemisphere – the European Large Area *ISO* Survey-North 1 and -North 2 regions (ELAIS-N1 and ELAIS-N2), and the Lockman Hole. A great deal of complementary data has been taken on the SWIRE fields; a band-merged catalogue containing over one million sources has been created (Data Release 2; Surace et al. 2005), and a photometric redshift catalogue has been generated (Rowan-Robinson et al. 2008) from the multi-wavelength data. All three northern regions are covered by the Faint Images of the Radio Sky at Twenty-cm (FIRST; Becker et al. 1995) and NRAO VLA Sky Survey (NVSS; Condon et al. 1998) 1.4-GHz surveys; however the relatively shallow sensitivity levels of these observations (0.75 and 2.25 mJy respectively) means that these surveys are dominated by classical radio galaxies, and contain few star-forming galaxies. We have been carrying out a series of deeper radio surveys of the northern SWIRE fields, in order to extend the multi-wavelength coverage currently available on star-forming galaxies into radio frequencies.

In Section 2 we present new observations of the ELAIS-N2 region, taken at 610 MHz with the Giant Metrewave Radio Telescope (GMRT; Ananthakrishnan 2005). We combine these observations with our previous surveys of the ELAIS-N1 and Lockman Hole regions (Garn et al. 2008a,b) in Section 3, and create a sample of 510 star-forming galaxies with photometric redshifts that are detected in the infrared and radio. In Section 4 we look at the infrared / radio flux density ratio q'_{IR} , and use deviations away from the typical values seen for star-forming galaxies to identify sources that may contain a significant excess of radio emission due to the presence of an active galactic nucleus (AGN). We compare our sample to the local relationship between radio luminosity and SFR given by Bell (2003), and find that the majority of sources are well described by

this relationship, but that there are a small fraction of sources where the SFR would be significantly under-estimated by using the radio luminosity. In Section 5 we test the assumption that the local relationship between SFR and radio luminosity can be used to calculate the SFRD of the Universe from galaxies at high redshift ($z = 2$), and from galaxies undergoing much more vigorous starbursts than are seen in the local Universe.

Throughout this work a flat cosmology with the best-fitting parameters from the Wilkinson Microwave Anisotropy Probe (WMAP) five-year data of $\Omega_{\Lambda} = 0.74$ and $H_0 = 72 \text{ km s}^{-1} \text{ Mpc}^{-1}$ is assumed (Dunkley et al. 2009).

2 RADIO OBSERVATIONS

2.1 The ELAIS-N2 region

The ELAIS-N2 region was observed in 2006 July 15 and 17 with the GMRT. Observations were made in two 16-MHz sidebands centred on 610 MHz, each split into 128 spectral channels, with a 16.9 s integration time. Thirteen pointings were observed, centred on $16^{\text{h}}36^{\text{m}}48^{\text{s}}$, $+41^{\circ}01'45''$ (J2000 epoch) and spaced by 36 arcmin in a hexagonal pattern, in a series of short interleaved scans in order to maximise the uv coverage. The typical time spent on each pointing was 22 min. A nearby phase calibrator, J1613+342, was observed for 4 min between every two or three target scans to monitor any time-dependent phase and amplitude fluctuations of the telescope. Flux density calibration was performed using observations of 3C48 or 3C286, at the beginning and end of each observing session. The task SETJY was used to calculate 610-MHz flux densities of 29.4 and 21.1 Jy respectively, using the Astronomical Image Processing Software (AIPS) implementation of the Baars et al. (1977) flux density scale.

Data reduction was performed in a similar way to our previous GMRT surveys (Garn et al. 2007, 2008a,b). Initial editing of the data took place separately on each sideband with standard AIPS tasks, to remove bad baselines, antennas, and channels which were suffering from large amounts of narrow band interference, along with the first and last integration periods of each scan. The flux calibrators were used to create a bandpass correction for each antenna. In order to create a pseudo-continuum channel, five central frequency channels were combined together, and an antenna-based phase and amplitude calibration created using observations of J1613+342. This calibration was applied to the original data, which was then compressed into 11 channels of bandwidth 1.25 MHz, small enough that bandwidth smearing was not a problem for our images. The first and last few spectral channels, which tended to be the noisiest, were omitted from the data, leading to an total effective bandwidth of 13.75 MHz in each sideband. Further flagging was performed on the 11-channel data set, and the two sidebands combined using UVFLP (Garn et al. 2007) to improve the uv coverage. Baselines shorter than 1 k λ were omitted from the imaging, since the GMRT has a large number of small baselines which would otherwise dominate the beam shape.

Each pointing was divided into 31 smaller facets, arranged in a hexagonal grid, which were imaged individually with a separate assumed phase centre. The large total area imaged (a diameter of $1^{\circ}8$, compared with the full width at half-maximum of the GMRT, which is $\sim 0^{\circ}74$) allows bright sources well away from the observed phase centre to be cleaned from the images, while the faceting procedure avoids phase errors being introduced due to the non-planar nature of the sky. All images were made with an elliptical restoring beam of size $6.5 \times 5 \text{ arcsec}^2$, PA $+70^{\circ}$, with a pixel size of

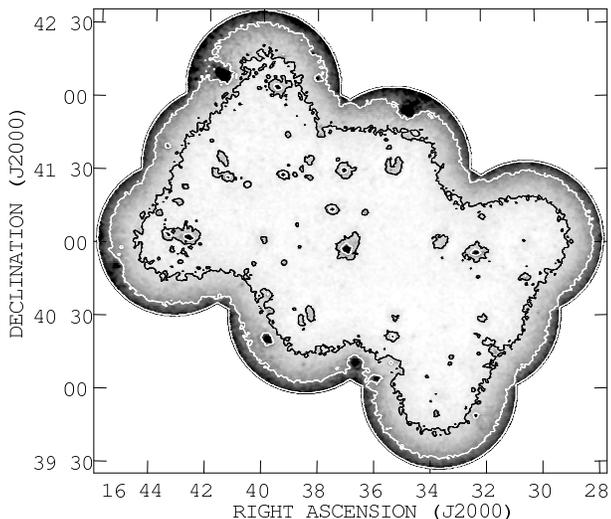


Figure 1. The rms noise map for the GMRT ELAIS-N2 survey. The grey-scale ranges between 80 and $400 \mu\text{Jy beam}^{-1}$, and the contour levels are drawn at 120 and $240 \mu\text{Jy beam}^{-1}$ (black and white lines respectively).

1.5 arcsec to ensure that the beam was oversampled. The images went through three iterations of phase self-calibration at 10 , 3 and 1 min intervals, and then a final round of self-calibration correcting both phase and amplitude errors, at 10 min intervals, with the overall amplitude gain held constant in order not to alter the flux density of sources.

The offset in the GMRT primary beam seen in our previous surveys was again detected and corrected, using the method described in Garn et al. (2007). The 13 pointings were mosaicked together, taking into account the offset primary beam and weighting the final mosaic appropriately by the relative noise of each pointing. The mosaic was cut off at the point where the primary beam correction dropped to 20 per cent of its central value, a radius of $0^{\circ}53$ from the centre of the outer pointings.

The rms noise for the individual pointings, before correction for the GMRT primary beam, was between 83 and $90 \mu\text{Jy beam}^{-1}$, compared with the expected noise level of $80 \mu\text{Jy beam}^{-1}$ (calculated using Equation 1 from Garn et al. 2007), and the rms noise map for the mosaic is shown in Fig. 1.

2.2 Observations of ELAIS-N1 and the Lockman Hole

610 -MHz GMRT observations of the ELAIS-N1 field (Garn et al. 2008a) and the central region of the Lockman Hole field (Garn et al. 2008b) have previously been presented. A brief summary of the observations is given here; for further details, the relevant papers should be consulted.

The ELAIS-N1 survey covers $\sim 9 \text{ deg}^2$ (the majority of the *Spitzer* observation region) with a resolution of $6 \times 5 \text{ arcsec}^2$, PA $+45^{\circ}$. The rms noise level of the majority of the survey was $\sim 70 \mu\text{Jy beam}^{-1}$ before primary beam correction, with a smaller ‘deep’ region having $\sim 40 \mu\text{Jy beam}^{-1}$ rms.

The Lockman Hole survey covers $\sim 5 \text{ deg}^2$, within the central area of the region observed by *Spitzer*. The survey resolution was $6 \times 5 \text{ arcsec}^2$, PA $+45^{\circ}$, and the noise level $\sim 60 \mu\text{Jy beam}^{-1}$ over the majority of the region, with a small area having significantly greater noise due to the presence of a nearby bright radio source.

3 DATA SELECTION

3.1 Creating an infrared sample

The infrared data comes from the band-merged SWIRE source catalogues of Surace et al. (2005), and the photometric redshift catalogue of Rowan-Robinson et al. (2008). In order to be included in the band-merged catalogue, sources were required to be detected above a signal-to-noise ratio (SNR) of 10 and 5 at $3.6 \mu\text{m}$ and $4.5 \mu\text{m}$ (approximately equivalent to $10 \mu\text{Jy}$ in both bands). There are fewer sources present in the photometric redshift catalogue than the band-merged catalogue, due to the need for sufficient spectral information that a redshift could be determined. Sources were required to be present in both the band-merged and photometric redshift catalogues, due to the need for a redshift, and the increased amount of information present in the band-merged catalogue. This provided information on infrared flux densities in the four IRAC bands, along with $24\text{-}\mu\text{m}$ and $70\text{-}\mu\text{m}$ flux densities, and five-band optical photometry ($Ug'r'i'Z'$) from the Wide Field Survey (WFS; McMahon et al. 2001; Irwin & Lewis 2001) for the ELAIS-N1 and ELAIS-N2 fields, with four-band ($Ug'r'i'$) photometry for the Lockman Hole from the SWIRE photometry program.

Sources must also be classified as ‘star-forming’, and have an estimate of the SFR. This classification and estimate comes from the template fitting performed by Rowan-Robinson et al. (2008) during their photometric redshift calculations, and rejects some sources that are identified as having their infrared energetics dominated by AGN activity. An infrared detection at both 24 and $70 \mu\text{m}$ is also required in order to constrain the thermal emission from dust, and to have sufficient information on the region of the infrared SED where the bulk of the bolometric energy output of star-forming galaxies is seen. Selecting galaxies at both 24 and $70 \mu\text{m}$ increases the accuracy of the infrared bolometric luminosity calculation performed by Rowan-Robinson et al. (2008), which would otherwise have a factor of ~ 2 uncertainty, and improves the accuracy of their SFR estimates. Finally, we require the sources to lie within the area that was observed in one of the GMRT radio surveys. The numbers of sources in each field that satisfy the selection criteria are given in Table 1.

3.2 Matching to the radio data

In creating the public catalogues for the ELAIS-N1 and Lockman Hole GMRT surveys, a two-stage selection criterion with an increased SNR requirement near to bright sources was implemented (for more details see Garn et al. 2008a) – this was due to problems encountered from residual phase errors near to the brightest radio sources in the survey. For this study, we have known source positions from the infrared and optical detections, and so relax this criterion to a SNR of 4 . Radio sources were matched to the infrared data if the source centres were within a distance r of each other – if there were potential multiple matches, the closest match was selected. There will be some incorrect associations between the infrared and radio catalogues – we estimated this value by shifting the coordinates of all radio sources by 10 arcmin in declination and seeing how many (incorrect) associations were then made at the same matching radius r . We required the false matching rate to be less than 5 per cent, which corresponded to $r = 2.5 \text{ arcsec}$. The number of galaxies with a radio detection within 2.5 arcsec are listed in Table 1, with a total of 510 galaxies in all three survey fields that satisfied the infrared and radio selection criteria.

Table 1. The number of sources in each sub-sample – see Sections 3.1 and 3.2 for further details on sample selection.

	ELAIS-N1	ELAIS-N2	Lockman Hole	Total
Infrared band-merged catalogue (Surace et al. 2005)	282711	126056	323044	731811
Infrared photometric redshift catalogue (Rowan-Robinson et al. 2008)	218117	125364	229238	572719
Band-merged and photometric catalogues	121422	61610	132736	315768
Star-forming sources only, with SFR estimate	49160	24831	42517	116508
Star-forming, and 24- μm detection	11371	5725	12458	29554
Star-forming, 24- μm and 70- μm detections	2470	1344	2939	6753
Star-forming, 24- μm and 70- μm detections, within radio coverage area	2204	1317	1891	5412
Star-forming, 24- μm and 70- μm detections, plus 610-MHz radio detection	279	63	168	510

3.3 Sample selection biases

We have rejected sources from the infrared-selected samples that were classified by Rowan-Robinson et al. (2008) as having optical and infrared photometry that is best fitted by an AGN template; however there are several examples of galaxies that undergo concurrent AGN and star formation activity (e.g. Richards et al., 2007; Norris, Middelberg & Boyle 2007) which will not necessarily be identified during this process, and this selection will not remove sources which have a significant contribution to their radio emission from AGN activity, but are not clearly AGN-like at shorter wavelengths. We return to the question of AGN contaminants in Section 4.1.

Selecting galaxies at both 24 and 70 μm places a significant restriction on the sample size, as seen in Table 1. Approximately 25 per cent of the star-forming galaxies with an estimate of SFR were detected in the 24- μm band, and of these galaxies, approximately 25 per cent were detected at 70 μm . The infrared emission at 24 μm is dominated by transiently heated polycyclic aromatic hydrocarbon (PAH) molecules (e.g. Léger & Puget 1984; Puget & Léger 1989; Draine 2003, and references therein) and is strongly related to the amount of ongoing star formation, while the emission at 70 μm is dominated by thermal emission from large dust grains. Both detections are considered necessary in order to be sure of the accuracy of the template fitting and SFR estimation.

Fig. 2a shows the redshift distribution of 24- μm selected galaxies. The bulk of galaxies are at $z < 0.5$, although there is a secondary peak at $z \sim 1$ due to the shifting of the 11.7- μm PAH feature into the 24- μm band (Rowan-Robinson et al. 2008). The 70- μm flux limit for the SWIRE surveys is significantly higher than the 24- μm limit (30 mJy compared with 0.45 mJy; Surace et al. 2005), and by selecting galaxies with 70- μm fluxes, the sample is biased towards galaxies that are brighter at mid-infrared wavelengths, and have high SFR. The secondary redshift peak at $z \sim 1$ is reduced in strength for the sample selected at 24- μm and 70- μm , but remains prominent – this is due to the global decrease in SFRD of the Universe, seen between $z \sim 2$ and the current day (e.g. Lilly et al. 1996; Madau et al. 1996; Hopkins & Beacom 2006), a consequence of which is that the highest SFR galaxies are likely to be found at higher redshift. The SFR distribution of the two samples is given in Fig. 2b, and shows that a greater fraction of galaxies in the 24- μm and 70- μm selected sample have $\text{SFR} \geq 100 M_{\odot} \text{ yr}^{-1}$ than when only a 24- μm detection is required. Fig. 3 illustrates that high-SFR sources are more likely to be found at higher z in our sample. The upper left of the diagram is relatively unpopulated due to the lower space density of high SFR sources in the local Universe compared to at $z \sim 2$, while the lower right of the diagram is unpopulated principally because of the flux limit of the 70- μm data

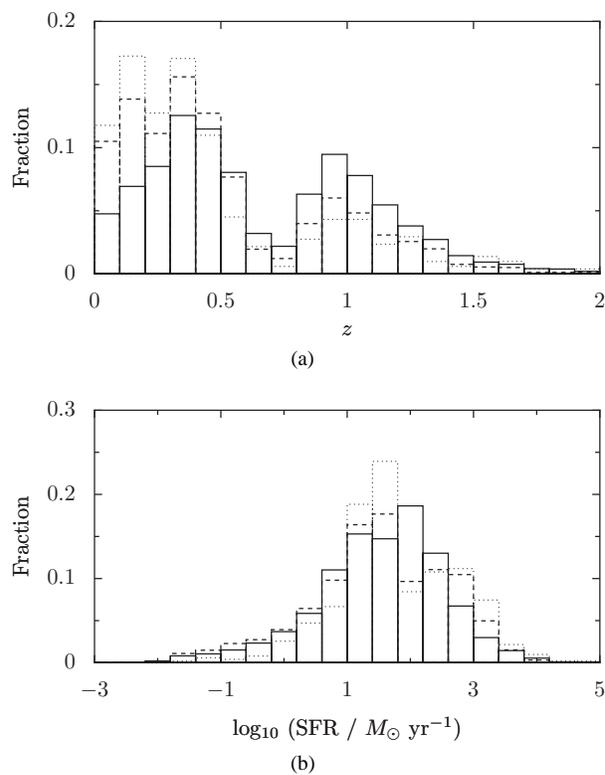


Figure 2. The fractional distribution of (a) redshift and (b) SFR for galaxies selected at 24 μm (solid line), 24 and 70 μm (dashed line), and 24 μm , 70 μm and 610 MHz (dotted line) – see Section 3.3 for further details.

used in the Rowan-Robinson et al. (2008) catalogue. The curved line indicates the minimum detectable SFR at different redshifts, based upon the 70- μm flux only, using the relationship between a monochromatic MIPS flux density and SFR given by Rieke et al. (2009). There are a few sources seen below this limit, due to the method used by Rowan-Robinson et al. (2008) to estimate SFRs (see Section 4.3.3), which considers more information than just a single 70- μm detection. Note that the shape of the SFR limit depends both on the intrinsic limiting luminosity for a flux-limited sample, and the k -correction caused by the slope of the mid-infrared SED for a typical starburst galaxy.

The photometric redshift catalogue of Rowan-Robinson et al. (2008) contains a considerable number of sources with an inferred SFR of $> 1000 M_{\odot} \text{ yr}^{-1}$. Such extreme SFRs are unusual, and for many sources are likely to be unphysical, but are not unknown (see, e.g. Capak et al. 2008, for a discussion of a spectroscopically-

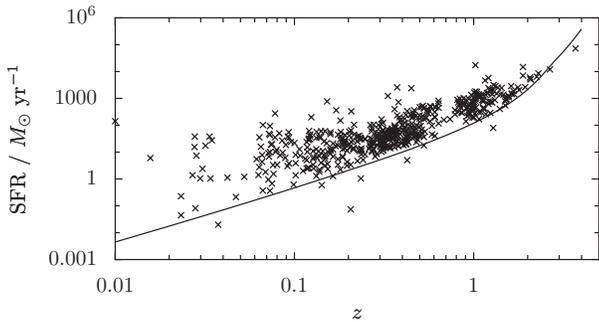


Figure 3. The relationship between z and SFR for the 510 galaxies detected at $24\ \mu\text{m}$, $70\ \mu\text{m}$ and $610\ \text{MHz}$. The solid line represents the limiting SFR detectable at different redshifts, using the relationship between monochromatic $70\text{-}\mu\text{m}$ flux density and SFR given by Rieke et al. (2009).

confirmed source with $\text{SFR} \sim 4000\ M_{\odot}\ \text{yr}^{-1}$). We note that SFRs derived from either $24\text{-}\mu\text{m}$ or $70\text{-}\mu\text{m}$ fluxes are consistent with these high values for most of the extreme SFR sources in our sample (see Section 4.3.3), although the greatest SFR that Rieke et al. (2009) model is $\sim 1600\ M_{\odot}\ \text{yr}^{-1}$, and inferred SFRs above this value will be very poorly constrained. We also note that SFRs derived independently from radio data are consistent with these high values (see Section 4.2), although in both cases an error in the calculated photometric redshift may be leading to a significant overestimation of the SFR. The small number of sources in our sample with a very high inferred SFR do not affect our later conclusions on variations in the relationship between radio luminosity and SFR with redshift.

Selecting galaxies with photometric redshifts, rather than requiring spectroscopic redshifts, improves the homogeneity of the sample – all galaxies with sufficient photometry will be included in the study, rather than limiting the sample to galaxies that are sufficiently bright at one wavelength that they were selected for spectroscopic followup. Photometric redshifts are inherently less accurate than spectroscopic equivalents – however, there were considerable numbers of spectroscopic redshifts available for validation in the SWIRE fields, and Rowan-Robinson et al. (2008) estimate an typical error of 4 per cent in $(z_{\text{phot}} - z_{\text{spec}})/(1 + z_{\text{spec}})$, with ~ 1 per cent of the photometric redshifts being catastrophically incorrect. Where both spectroscopic and photometric redshifts are available, we use the spectroscopically determined value, and we return to the possibility of catastrophic redshift errors in Section 4.3.3.

The radio surveys used in this work are much less sensitive to star-forming galaxies than the infrared surveys, as can be seen by the low number of source detections in the bottom row of Table 1. The percentage of infrared-selected galaxies that are detected at $610\ \text{MHz}$ is 4.8 per cent (ELAIS-N2), 8.9 per cent (Lockman Hole) and 12.7 per cent (ELAIS-N1), with the fields that have lower 610-MHz noise levels having a greater percentage of source matches. Due to the positive correlation that is seen between radio luminosity and SFR (e.g. Condon & Yin 1990; Bell 2003, and see Section 4.2), additionally requiring a detection at $610\ \text{MHz}$ will bias the sample against galaxies with very low SFR. This can be seen in Fig. 2b – the fraction of galaxies with $\text{SFR} < 1\ M_{\odot}\ \text{yr}^{-1}$ is significantly reduced compared with the infrared-only samples. A study of sources below the radio detection limit, requiring a statistical process such as median source stacking (e.g. Boyle et al. 2007; Beswick et al. 2008), is beyond the scope of this paper, but has been discussed

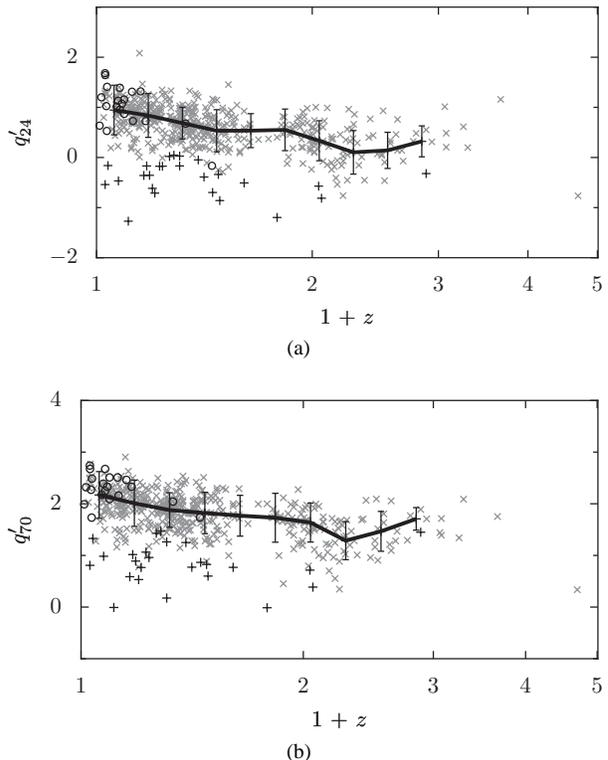


Figure 4. Variation in (a) q'_{24} and (b) q'_{70} with redshift, along with the local median value of q'_{IR} (black line with error bars). Sources which have been identified as being AGN-like from their deviation below the median value of q'_{24} are indicated by crosses, ‘+’ – see Section 4.1 for further details. Open circles, ‘o’, mark the sources that have been identified as being radio-quiet compared with their SFR – see Section 4.3 for further details.

in a separate work (Garn & Alexander 2009). We will return to the galaxies where a non-detection in the radio is significant in Section 4.3.

4 RESULTS

4.1 Identifying potential AGN contaminants

There is a tight relationship between the infrared and radio luminosities of galaxies that are predominantly powered by star-formation processes (the ‘infrared / radio correlation’; e.g. Helou et al. 1985; Condon et al. 1991; Murphy et al. 2006), which is not followed by sources that have significant amounts of AGN activity (Sopp & Alexander 1991; Roy et al. 1998). The correlation has previously been used as a discriminant between the two types of source (e.g. Ibar et al. 2008; Seymour et al. 2008), and in order to use this technique on our sample, we consider the monochromatic q'_{IR} parameter given by

$$q'_{\text{IR}} = \log_{10} \left(\frac{S_{\text{IR}}}{S_{610}} \right), \quad (1)$$

where S_{IR} is the infrared flux density in either the $24\text{-}\mu\text{m}$ or $70\text{-}\mu\text{m}$ bands, and S_{610} is the radio flux density at $610\ \text{MHz}$. Note that this definition is slightly different from previous works (e.g. Appleton et al. 2004) which typically use 1.4-GHz flux densities. Fig. 4 shows the variation in q'_{24} and q'_{70} with redshift for the galaxies in this sample. The dispersion in the individual q'_{IR} values is

greater than typically seen at 1.4 GHz (Appleton et al. 2004). The principal reason for this is that for galaxies which have *both* AGN and star-forming activity, the 610-MHz flux density mainly stems from the nuclear source, while the 1.4-GHz flux density comes mainly from star formation activity (Magliocchetti et al. 2008). AGNs were identified by finding sources that were a better fit to the selected AGN templates of Rowan-Robinson et al. (2008) than to elliptical galaxy templates, as discussed in Section 3; these were then removed from the sample. Any sources that have their radio luminosity dominated by an AGN, but do not clearly show up as having infrared AGN templates, will not have been removed through this method. These ‘missed’ AGN sources will be radio bright, and therefore have a low value of q'_{IR} .

We have not converted the data in Fig. 4 to a consistent rest-frame wavelength (a ‘ k -correction’), and so the observed value of q'_{IR} will vary with the redshift of the galaxy, as different portions of the redshifted SED enter into our observation bands. In order to quantify how the typical value of q'_{IR} varies, we calculate the median value of q'_{IR} in ten logarithmically-spaced redshift bins between $z = 0$ and 2, and show this as the solid line in Fig. 4, along with error bars indicating the local standard deviation σ . The median value of q'_{IR} shows a steady decline with redshift at both 24 and 70 μm , due to the shape of a typical galaxy SED, which has a steeper spectrum in the mid-infrared than in the radio. We define sources which have a value of q'_{24} below the local median value by more than 2σ to be ‘AGN-like’ – the typical value of σ for a bin is 0.4, making these sources a factor of ~ 6 more radio-bright than is typical. This criterion is similar to that used by Ibar et al. (2008), although they used 2σ below the mean value of q'_{24} as their cut-off value. The median estimator is more robust to the presence of outliers than the mean; since it is these outliers which we are trying to identify, the median is a more appropriate statistic to use. There are 25 sources out of 510 (5 per cent) which satisfy this criterion, seven of which are more than 3σ away from the local median. The AGN-like sources are identified in Fig. 4. For comparison, there are only five sources that lie above the median value of q'_{24} by more than 2σ , and none by more than 3σ . A similar selection for AGN-like sources could be made in terms of differences from the median value of q'_{70} – however, most of the sources that show significant deviations at 70 μm have already been identified through their q'_{24} deviation, and since the resolution of the 24- μm data is a much better match to the 610-MHz data we choose to consider deviations from q'_{24} only.

All of the AGN-like sources were visually inspected in the radio images, in order to look for extended jet/lobe structure. One source was potentially the central nucleus of an extended radio source, but none of the other sources showed evidence for any extended radio structure. Fig. 5 shows optical, IRAC and MIPS 50×50 arcsec² images centred on each of the AGN-like sources. The sources are typically compact, although a few (e.g. the fourth source on the top row of Fig. 5) show signs of extended emission in the optical images. Throughout the rest of this work, the AGN-like sources will be retained in the sample, but identified as potential contaminants in order to compare them to the remainder of the population.

4.2 Star formation rate estimates

The SFR estimates for the galaxies in our sample come from the SED fitting and photometric redshift estimation of Rowan-Robinson et al. (2008). A further method of estimating the SFR, Ψ , from the 1.4-GHz luminosity of galaxies is described by

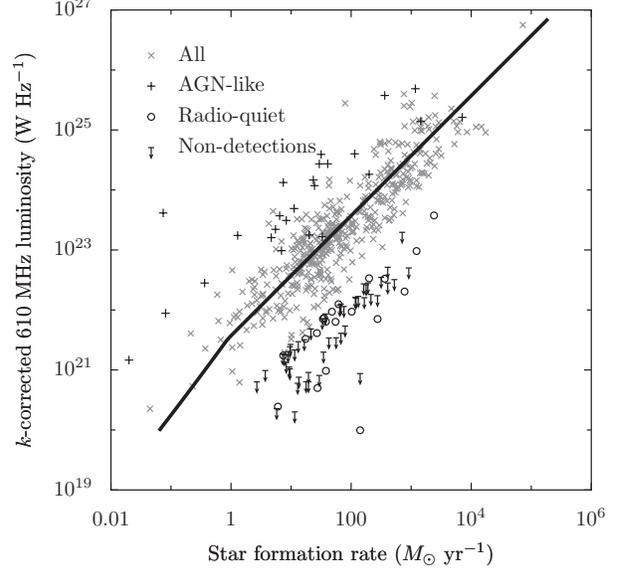


Figure 6. The relationship between k -corrected 610-MHz radio luminosity and SFR (grey diagonal crosses) and the prediction of Bell (2003) shifted to 610 MHz assuming $\alpha = 0.8$ (solid line). The sources identified as AGN-like are shown as crosses, ‘+’, and the sources identified as being radio-quiet (see Section 4.3) are shown as open circles, ‘o’. Significant non-detections are indicated by upper limits – see Section 4.3 for further details.

Bell (2003), calibrated from the total infrared SFR for galaxies with $L \geq L_*$ (defined as having an infrared luminosity $L_{\text{IR}} \sim 2 \times 10^{10} L_{\odot}$). Assuming a radio spectral index $\alpha = 0.8$ (e.g. Condon 1992), where we define α such that the flux density $S = S_0 \nu^{-\alpha}$, we convert this relationship to a 610-MHz equivalent:

$$\left(\frac{\Psi}{M_{\odot} \text{yr}^{-1}} \right) = 2.84 \times 10^{-22} \left(\frac{L_{610}}{\text{W Hz}^{-1}} \right) \quad (2)$$

for $L_{610} > L_c$ (where $L_c = 3.3 \times 10^{21} \text{ W Hz}^{-1}$ is the luminosity at 610 MHz of a $\sim L_*$ galaxy, with $\Psi \simeq 1 M_{\odot} \text{yr}^{-1}$), and

$$\left(\frac{\Psi}{M_{\odot} \text{yr}^{-1}} \right) = \frac{2.84 \times 10^{-22}}{0.1 + 0.9(L_{610}/L_c)^{0.3}} \left(\frac{L_{610}}{\text{W Hz}^{-1}} \right) \quad (3)$$

for $L_{610} \leq L_c$.

Fig. 6 shows the relationship between 610-MHz radio luminosity and SFR. The radio data were k -corrected from an observation-frame flux density into a rest-frame luminosity using

$$L_{610} = 4\pi d_L^2 S_{610} (1+z)^{\alpha-1}, \quad (4)$$

where we assume that $\alpha = 0.8$, and where d_L is the luminosity-distance corresponding to redshift z . The relationship given by Equations 2 and 3 is overlaid on the data, and shows a very good agreement with the overall trend for sources which are detected in the radio images. Because the sample has few galaxies with SFR less than $1 M_{\odot} \text{yr}^{-1}$, we are unable to confirm the existence of a break at $L < L_c$. The sources that were previously identified as AGN-like all have a higher radio luminosity than predicted by Equation 2 (which applies to star-forming galaxies only), although some do not deviate far from the overall trend.

We define the ratio of L_{610}/Ψ to be the ‘specific radio luminosity’ of a galaxy, and calculate the median value of $\log_{10}(L_{610}/\Psi)$, for all sources with radio detections, and for sources with SFR $\geq 1 M_{\odot} \text{yr}^{-1}$ which are not classified as being AGN-like. The medians and standard deviations are 21.51 ± 0.61

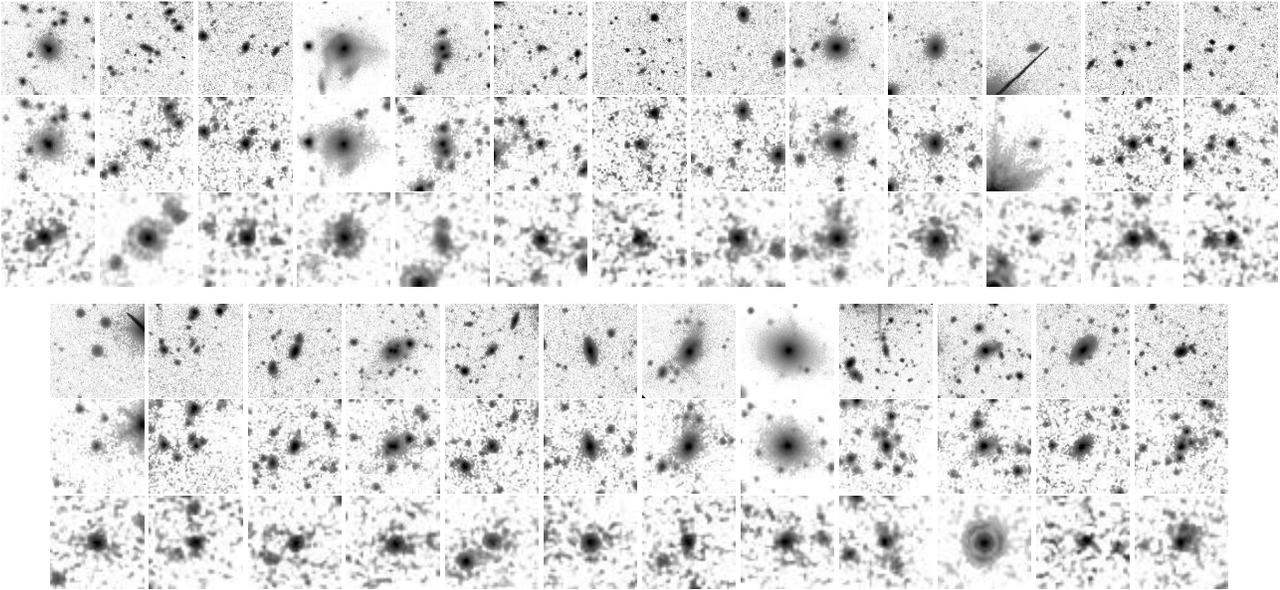


Figure 5. Optical and infrared images of the 25 AGN-like sources, retrieved from the NASA/IPAC infrared science archive. All images are 50×50 arcsec² in size. Top row: r' -band images. Middle row: 3.6- μ m images. Bottom row: 24- μ m images.

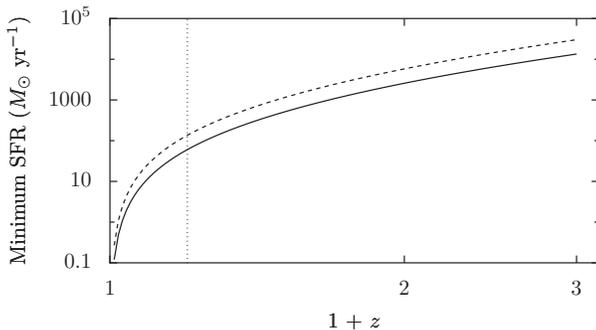


Figure 8. The minimum SFR necessary for sources to be identified as radio-quiet, based upon 610-MHz noise levels of $40 \mu\text{Jy beam}^{-1}$ (solid line) and $90 \mu\text{Jy beam}^{-1}$ (dashed line). The vertical dotted line indicates a redshift of 0.2.

and 21.48 ± 0.55 respectively, consistent with the Bell (2003) value (shifted to 610 MHz) from Equation 2 of 21.55. In contrast, the radio-luminosity / SFR relationship given by Condon & Yin (1990), which is based around the ratio of the non-thermal Galactic luminosity at 408 MHz and an estimate of the Galactic supernova rate, predicts a value of 21.17 at 610 MHz – also within one standard deviation of our results, but a less good fit to the observations.

4.3 Radio-quiet sources

There are several sources which are detected in the radio images, but show significantly lower values of radio luminosity in Fig. 6 than would be expected from their SFR and Equation 2. We define ‘radio-quiet’ sources as having a value of $\log_{10}(L_{610}/\Psi)$ that is at least 2σ below the median value, calculated from non-AGN sources only. There are 20 sources satisfying this criterion, which are marked as such on Fig. 6. The sources are at low redshift (see Fig. 4), with 90 per cent being at $0 < z < 0.2$.

As discussed in Section 3.3, the *Spitzer* surveys are more sen-

sitive to star-forming galaxies than the radio surveys – of the 5412 infrared-selected sources, only 510 were detected at 610 MHz. In order to identify which of the non-detections are significant, we determine upper limits on 610-MHz flux density for each source, based upon four times the local noise level, and place upper limits on the radio luminosity using Equation 4. We then determine an upper limit on the value of $\log_{10}(L_{610}/\Psi)$ using the Rowan-Robinson et al. (2008) SFR values – for the majority of sources, this value lies above or within the distribution of detected sources shown in Fig. 6 (i.e. the radio surveys are not deep enough to detect the source if it has a ‘typical’ specific radio luminosity); we consider these non-detections to be insignificant, and do not discuss them further. There remain a small number of sources which have an upper limit on specific radio luminosity that is more than 2σ below the value predicted by Equation 2 (i.e. we would expect to detect these sources if they had a ‘typical’ specific radio luminosity). There are 48 significant non-detections, which are shown on Fig. 6, and appear to be similar to the ‘radio-quiet’ sources previously identified.

There are a few potential explanations for these sources, which we consider in turn:

- (i) we have significantly under-estimated the radio luminosity for these sources (Section 4.3.1);
- (ii) the sources are genuinely radio-quiet, either due to a recent burst of star formation, or due to a suppression of the radio luminosity within these galaxies (Section 4.3.2);
- (iii) the SFR has been significantly over-estimated by Rowan-Robinson et al. (2008) (Section 4.3.3).

4.3.1 Under-estimation of the radio luminosity

Any significant under-estimation of the radio flux density would lead to a lower calculated value of the specific radio luminosity of galaxies. We inspected all of the radio-quiet sources in the radio images in order to test whether the radio counterparts were close to bright sources, or in noisy parts of the image, but no system-

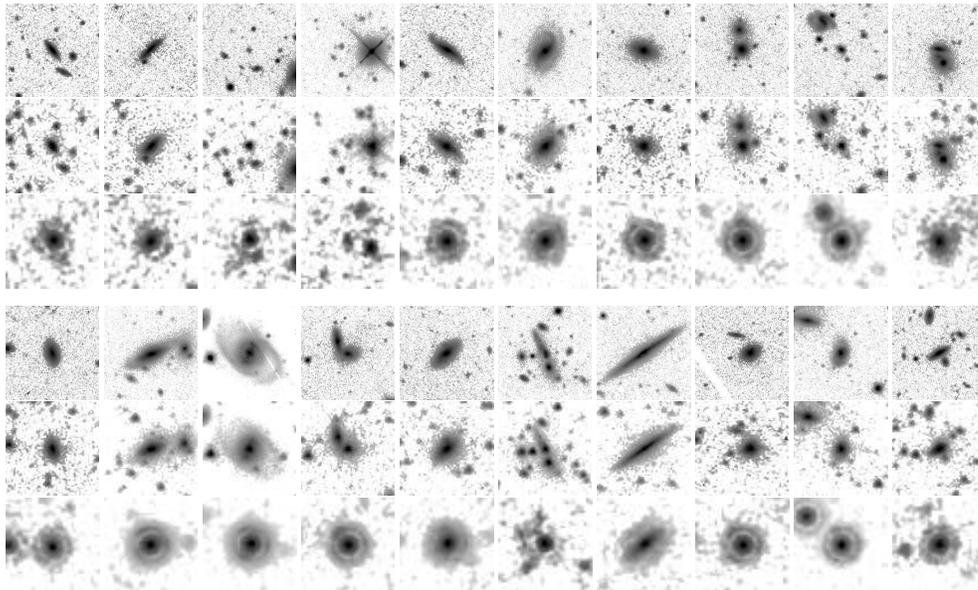


Figure 7. Optical and infrared images of the 20 radio-quiet sources, retrieved from the NASA/IPAC infrared science archive. All images are 50×50 arcsec² in size. Top row: r' -band images. Middle row: $3.6\text{-}\mu\text{m}$ images. Bottom row: $24\text{-}\mu\text{m}$ images.

atic effects were apparent. The sources are mainly at low redshift (90 per cent of the radio-quiet galaxies, and 94 per cent of the significant non-detections are at $0 < z < 0.2$), and galaxies are likely to have a greater angular size in the local Universe than at higher redshift. Fig. 7 shows that some of the radio-quiet sources appear to be extended in the optical and infrared images, suggesting that there may be diffuse radio emission near to or below the noise level which has not been included into the measured value of flux density.

The low redshift of these sources can be explained purely through selection effects – the SFR that is required for a source to be identified as either radio-quiet or as a significant non-detection depends on both the redshift of the source and the local noise level of the radio image, as illustrated by Fig. 8. At $z = 0.2$, a galaxy needs to have a SFR of at least $60 M_{\odot} \text{ yr}^{-1}$ to be classified as radio-quiet in the most sensitive portion of the ELAIS-N1 image, with noise level of $40 \mu\text{Jy beam}^{-1}$, or alternately a SFR greater than $135 M_{\odot} \text{ yr}^{-1}$ for a noise level of $90 \mu\text{Jy beam}^{-1}$, more characteristic of the ELAIS-N2 survey. Fig. 2b shows that most of the $24\text{-}\mu\text{m}$ and $70\text{-}\mu\text{m}$ selected sources have SFRs below these values, and so could not be identified as being significantly radio-quiet.

Even if the host galaxy is extended, the majority of star formation in high SFR galaxies tends to come from a nuclear starburst (e.g. Kennicutt 1998), and the bulk of the radio emission would not be expected to be spread out over a large area. In order to test for extended radio emission we measured the flux density of each of these sources within a circular aperture centred on their known location, using the technique described in Garn & Alexander (2009), and calculated the ratio of flux density measured within the aperture to the flux density listed in the catalogue. For the full sample of sources, the flux density measured within apertures of varying sizes was comparable to the catalogued flux density, from which we conclude that most of the sources have little extended radio emission. The AGN-like sources also follow this trend, but the radio-quiet galaxies show evidence for a slight increase in flux density within apertures of $\gtrsim 15$ arcsec radius, implying the existence of some diffuse radio emission which has not been catalogued. The increase is

less than a factor of two; this is not a large enough effect to make these galaxies significantly radio-quiet.

The conversion between flux density and luminosity relies upon an assumed radio spectral index of 0.8 for all sources; without multi-frequency radio data it is not possible to estimate this value more accurately. Garn et al. (2007) demonstrate that the spectral index distribution of galaxies detected at both 610 MHz and 1.4 GHz peaks around $\alpha = 0.8$, and various studies (e.g. Bondi et al. 2007; Ibar et al. 2009) have concluded that there is no significant variation in the mean spectral index of radio sources at flux densities down to $\sim 100 \mu\text{Jy}$. Even for an extreme error in the spectral index of $\sigma_{\alpha} = 0.5$, for a galaxy at $z = 2$, the inferred luminosity would not change by more than a factor of two; again, this is not a large enough effect to explain the radio-quietness of these sources.

4.3.2 Physical effects

There are a few potential reasons why galaxies could be radio-quiet with respect to their SFR; recent star-burst activity, or suppression of the radio luminosity due to a low confinement of cosmic rays, potentially caused by low magnetic field strengths. If a galaxy had just begun a burst of star formation activity that has enhanced the SFR, but not yet enhanced the supernova rate, it would appear to be radio-quiet – since the supernova rate lags the SFR by ~ 30 Myr (the approximate lifetime of $8 M_{\odot}$ stars), this would mean that sources were being observed very close to the beginning of the starburst period. Some of the sources (e.g. the second source in row two of Fig. 7) show signs of potential on-going mergers in their optical images, which would be an indication of triggered star formation, although this is not the case for all sources. A full analysis of the possibility of mergers in the sample is beyond the scope of this paper, although it seems unlikely that all of the radio-quiet sources in our sample could be undergoing merger activity.

The best-studied starburst galaxy in the local Universe is Arp 220, at $z = 0.018126$ (de Vaucouleurs et al. 1991) with SFR of $240 M_{\odot} \text{ yr}^{-1}$, calculated from its FIR luminosity (Sanders et al. 2003) and the relationship given in Kennicutt (1998). It has a 1.4-

GHz flux density of 0.326 Jy (Condon et al. 2002) and a 365-MHz flux density of 0.435 mJy (Douglas et al. 1996), giving it a spectral index $\alpha \simeq 0.2$. This equates to a luminosity of $2.5 \times 10^{23} \text{ W Hz}^{-1}$ at 610 MHz, and a ratio of $\log_{10}(L_{610}/\Psi)$ of ~ 21 , within 1σ of the median value found in Section 4.2, thus Arp 220 would not have been identified as being radio-quiet through this diagnostic. However, this should not be surprising – Arp 220 has a large number of compact radio sources visible (e.g. Smith et al. 1998; Lonsdale et al. 2006) which are thought to be radio supernovae formed due to the starburst activity – this system has therefore already passed the phase at which it could be identified as radio-quiet. The findings of Wilson et al. (2006) agree with this interpretation – there are a number of star clusters with ages up to around 500 Myr within Arp 220, suggesting that starburst activity started a long time ago. Any starburst galaxies identified through this diagnostic would have to be significantly earlier on in their starburst phase than Arp 220.

Carilli et al. (2008) have identified evidence for a possible decrease in the conversion factor between radio luminosity and SFR for high redshift ($z \sim 3$) Lyman break galaxies, based upon a stacking analysis of sources in the COSMOS field (although see Garn & Alexander 2009, for a discussion of the biases present in radio stacking experiments). Their favoured explanation of increased relativistic electron cooling due to inverse Compton scattering off the cosmic microwave background (CMB) would not apply to our low-redshift radio-quiet galaxies, since the energy density in the CMB increases with redshift as $(1+z)^4$ and is comparatively unimportant in the local Universe. A potential explanation for low-redshift radio-quiet sources would be that they have lower magnetic field strengths than is typical, leading to a decreased electron confinement (for the optically-thin scenario discussed by Chi & Wolfendale 1990) and a lower fraction of the total energy in cosmic rays being radiated within a galaxy compared with a source having a greater B -field. However, the radio-quiet sources follow the same infrared-radio correlation as the main sample (shown by Fig. 4) and a decrease in radio luminosity would therefore also require a corresponding decrease in the infrared luminosity; if this were the case, the measured SFR (which was calculated from the infrared luminosity) should also decrease, and sources would not be identified as being radio-quiet.

4.3.3 Over-estimation of the star formation rate

The SFR for these galaxies has been estimated using a complex method, described in Rowan-Robinson et al. (2008):

(i) optical and IRAC fluxes are used to find the best-fitting template spectrum for each galaxy, from a selection of six templates, and photometric redshifts are calculated;

(ii) sources with an ‘infrared excess’ at $\lambda \geq 8 \mu\text{m}$ have their bolometric infrared luminosity L_{IR} estimated from the long wavelength data;

(iii) 60- μm luminosities, L_{60} , are calculated from L_{IR} , using bolometric correction factors of 3.48, 1.67 and 1.43 for cirrus, M82 and Arp 220 galaxy templates respectively.

(iv) SFRs are then estimated from the 60- μm luminosity, using the conversion factor of

$$\left(\frac{\Psi}{M_{\odot}\text{yr}^{-1}}\right) = 2.2\epsilon^{-1}10^{-10}\left(\frac{L_{60}}{L_{\odot}}\right), \quad (5)$$

where ϵ describes the fraction of UV light absorbed by dust, and is taken to be 2/3.

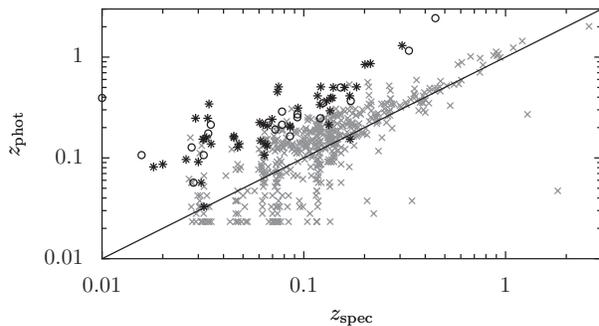


Figure 9. Comparison of spectroscopic and photometric redshifts for all galaxies in our 24- μm and 70- μm selected sample with spectroscopy (grey diagonal crosses), the radio-quiet sources (open circles) and the significant non-detections (stars). The 1:1 line is indicated for reference.

Rowan-Robinson et al. (2008) estimate an uncertainty in the total infrared luminosity at $z = 0.2$ (the approximate redshift of the radio-quiet sources) of 0.2 dex – this is too small to be responsible for the deviations which are seen. A more plausible scenario is for source confusion to play an important role – the resolution at 70 μm is only ~ 18 arcsec, much poorer than in the optical, IRAC or 24- μm bands. If there are two distinct sources present in the optical images, only one of which has been assigned a far-infrared counterpart (with the combined infrared flux from both) then that source will have its SFR overestimated in the photometric redshift catalogue, while the other source will not appear in the sample due to its lack of an infrared detection. Inspection of Fig. 7 shows several sources where confusion could potentially be having an effect on the SFR estimation. However, it could only plausibly increase the flux density by a factor of ~ 2 , and is not likely to lead to an order of magnitude discrepancy.

The conversion between L_{IR} and L_{60} has uncertainties in it, but again there is only a factor of ~ 2 difference between the three templates that are used. Likewise, the parameter ϵ used to calculate the amount of young star formation could be in error for galaxies with a significant old stellar population (Bell 2003; Rowan-Robinson 2003) which would lead to an over-estimation of the SFR, but neither of these factors could explain such a large difference in SFR for these sources.

The fact that the radio-quiet sources follow the same infrared / radio correlation as the main sample, but yet show a disagreement between their radio luminosity and infrared-derived SFR implies that the template-fitting carried out by Rowan-Robinson et al. (2008) to estimate photometric redshifts and total infrared luminosity may have been unsuccessful for a small number of sources – if this were the case, then the values of SFR derived from this process would be inaccurate. In order to test for this, in Fig. 9 we compare the photometric and spectroscopic redshifts for all of the galaxies which have available spectroscopy, and were selected at 24 and 70 μm . All 20 of the radio-quiet sources, and 46 of the 48 significant non-detections have spectroscopic redshifts, in contrast to the fraction of spectroscopic redshifts available for the whole sample (576/5412; 11 per cent). The Rowan-Robinson et al. (2008) criterion for defining a catastrophic redshift error is $\Delta\log_{10}(1+z) = \pm 0.06$, or 15 per cent; of the 66 radio-quiet or significant non-detected sources with spectroscopic redshifts, 30 (45 per cent) were outside this threshold. In contrast, only four of the sources which were detected at 610-MHz and not found to be radio-quiet were classified as having a catastrophic redshift error. We exclude these

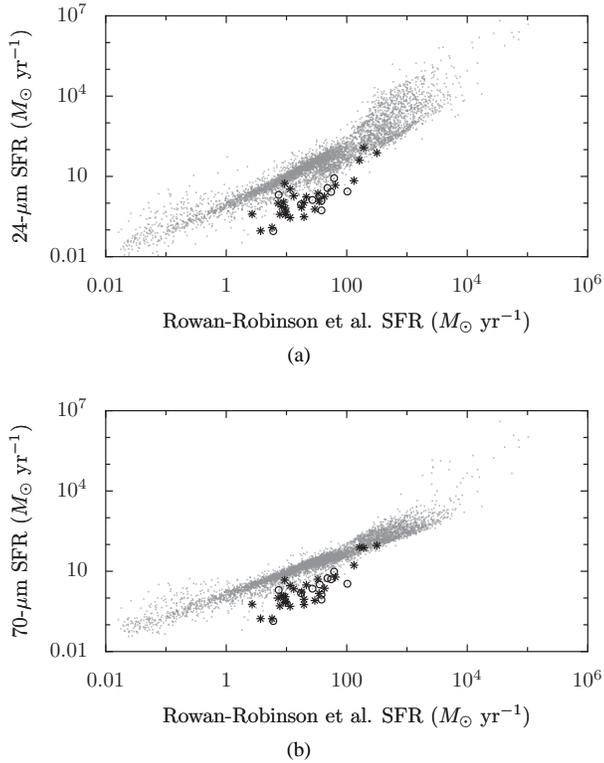


Figure 10. The relationship between SFRs estimated by the template-fitting of Rowan-Robinson et al. (2008), and SFRs estimated from the relationships given in Rieke et al. (2009), using (a) 24- μm flux densities; (b) 70- μm flux densities. Galaxies in the 24- μm and 70- μm -selected sample are shown as grey dots, with the radio-quiet sources indicated by open circles, and the significant non-detections shown as stars.

34 sources from the remainder of the analysis, as the SFRs calculated using inaccurate templates will be unreliable.

In order to test whether the SFRs for the remainder of the radio-quiet and significant non-detected sources are reliable, we use relationships provided by Rieke et al. (2009) to calculate SFRs directly from monochromatic flux densities measured by MIPS at either 24 or 70 μm . While SFRs based around a single flux measurement are likely to be less accurate than SFRs based around bolometric luminosities, Rieke et al. (2009) believe that they should be accurate to within about 0.2 dex, and these estimates can be used as an independent verification of the accuracy of the Rowan-Robinson et al. (2008) SFRs. In Fig. 10 we compare these three SFR estimates for our 24- μm and 70- μm selected sample. There is some scatter in the data, but it is clear that the galaxies which are radio-quiet or significant non-detections are typically outliers, with their monochromatic SFRs being smaller than the estimates from Rowan-Robinson et al. (2008).

We favour an over-estimation of the SFR in a small fraction of our sample for explaining the apparent low specific radio luminosity of a few of the sources, although we can not rule out a contribution from the other possibilities. We note that if SFRs calculated from either monochromatic 24- μm or 70- μm flux densities were used instead of the Rowan-Robinson et al. (2008) values for these sources, only two of the significant non-detections would remain significant, and none of the radio-quiet sources would still be classified as such. For completeness the radio-quiet sources and sources with a significant non-detection, which have not been re-

jected for poor template-fitting, will be retained on future plots for comparison with the rest of the population.

5 DISCUSSION

Bell (2003) presented a relationship between the SFR and 1.4-GHz non-thermal radio luminosity of galaxies in the local Universe. This was calibrated from local galaxies, assuming a direct proportionality between non-thermal radio emission and SFR for galaxies with $L_{\text{IR}} > L_*$. By constructing a sample of galaxies within the northern SWIRE regions, we have demonstrated that this relationship can be successfully applied to galaxies that are detected at 610 MHz. We compared the 610-MHz radio luminosity (k -corrected assuming a synchrotron radio spectrum with $\alpha = 0.8$) to the SFR in order to calculate a parameter, L_{610}/Ψ , which we call the ‘specific radio luminosity’ of star-forming galaxies. This value shows good agreement with the relationship given by Bell (2003), and a less good match to the more commonly-used relationship of Condon & Yin (1990). We find that approximately 4 per cent of the detected sources do not follow this relationship, and note the existence of several more galaxies that would be expected to be detected at 610 MHz, but also appear radio-quiet. Of the total number of 24- μm and 70- μm selected galaxies which could potentially be detected at 610 MHz, we find 12 per cent (68/558) are significantly more radio-quiet than the Bell (2003) relationship would suggest from their SFRs. We suggest a number of potential explanations for these sources, and favour an inappropriate conversion between infrared flux densities and SFRs for a small number of galaxies, due to an uncertainty in the photometric redshift calculations, rather than a real physical effect.

Various studies appear to indicate that there has been little evolution in the infrared / radio correlation at high redshift (e.g. Garrett 2002; Appleton et al. 2004; Ibar et al. 2008), suggesting that there has been little change in the physical processes which link star formation, thermal dust emission and radio luminosity, although these studies work with sources selected in the radio and are therefore biased against radio-quiet galaxies. In this work we do not directly test for variations in the luminosity correlation with redshift. However, the SFR estimates provided by Rowan-Robinson et al. (2008) allow a probe of any evolution in the physical link between SFR and radio synchrotron luminosity at high redshift, which has the advantage over studies which look at either the luminosity or flux density correlation in that we are working with one physical parameter (the SFR) and one potentially variable process (synchrotron radiation), rather than two processes (thermal dust emission at a given wavelength and synchrotron radiation) that could both vary with redshift.

In Fig. 11 we show the specific radio luminosity of the galaxies in our sample, as a function of redshift. Any variation seen in specific radio luminosity with z would suggest a change in one or more of the properties that controls the synchrotron radiation from star-forming galaxies – specifically, the galactic magnetic field strength, or the amount of confinement of the high-energy electrons. However, no such variation is seen – the majority of galaxies which are detected in the radio follow the global relationship given by Bell (2003) out to a redshift of at least 2 (a look-back time of 10.3 Gyr) and potentially to $z \sim 3$. The AGN-like sources discussed in Section 4.1 all have a high specific radio luminosity (which is to be expected if some of their radio luminosity is not related to star formation activity), but their specific radio luminosity shows no evidence for redshift evolution. The radio-quiet sources discussed in

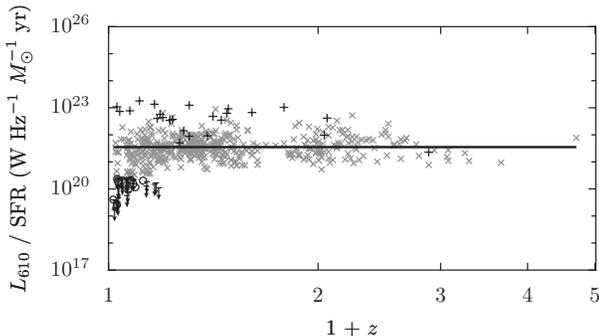


Figure 11. The relationship between 610-MHz radio luminosity and SFR, as a function of redshift – symbols are the same as for Fig. 6. The local relationship given by Bell (2003) is indicated by the solid line – there is no evidence for variation in the radio luminosity / SFR relationship out to $z = 2$, for radio-selected star-forming galaxies.

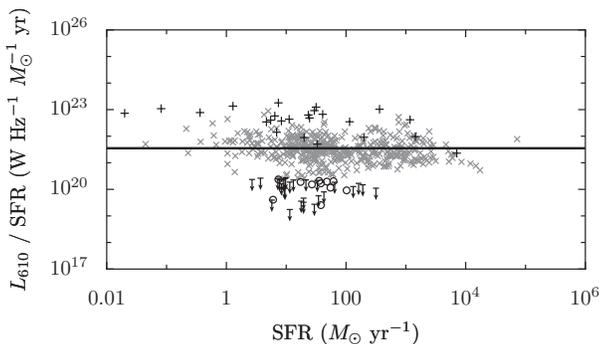


Figure 12. The relationship between 610-MHz radio luminosity and infrared-derived SFR, as a function of SFR – symbols are the same as for Fig. 6. The relationship given by Bell (2003) is indicated by the solid line.

Section 4.3 all lie at low redshift and do not affect this conclusion, although we caution that due to selection effects, we are unable to test for the existence or the number of radio-quiet sources which may exist at redshifts beyond 0.2.

As discussed in Section 1, there is much interest in trying to calculate the star formation history of the Universe. Radio observations at ~ 1 GHz are unaffected by dust, and should allow a reliable estimation of the variation in SFRD with z , without the uncertainties that are found at optical and infrared wavelengths. There have been a few attempts to carry out this calculation (e.g. Mobasher et al. 1999; Haarsma et al. 2000; Seymour et al. 2008; Smolčić et al. 2009) but all of these rely upon the untested assumption that the local relationship between radio luminosity and SFR can be applied successfully at higher redshift. The work presented here demonstrates that this assumption is valid – the radio luminosity of the majority of radio-selected star-forming galaxies does track the SFR out to at least $z = 2$ (with some potential evidence of an extension out to $z \sim 3$ and beyond; see Fig. 11).

Equally importantly, the relationship between luminosity and SFR has been implicitly assumed to be the same for galaxies with all values of SFR. Fig. 12 shows that, at least over the range $1 - 10^4 M_{\odot} \text{ yr}^{-1}$, no significant variation in this relationship is seen. Galaxies undergoing extreme starbursts, with SFRs up to $10^4 M_{\odot} \text{ yr}^{-1}$, and galaxies undergoing much lower star-formation activity with SFR of $1 M_{\odot} \text{ yr}^{-1}$ show the same relationship be-

tween their synchrotron emission and SFR. The deviation predicted by Bell (2003) below $\sim 1 M_{\odot} \text{ yr}^{-1}$ cannot be tested in this work, due to a lack of low-luminosity sources in the sample.

We have demonstrated that the Bell (2003) relationship between 1.4-GHz luminosity and SFR (for $L \geq L_*$ galaxies) can be used successfully on galaxies at $0 < z < 2$, although it is necessary to first apply a k -correction to the observed flux density of a galaxy in order to convert to a rest-frame 1.4-GHz luminosity. Equation 6 gives a generalised version of this relationship, obtained through combining the Bell (2003) equation with Equation 4,

$$\left(\frac{\Psi}{M_{\odot} \text{ yr}^{-1}} \right) = \frac{0.066}{1+z} \left(\frac{d_L(z)}{\text{Mpc}} \right)^2 \left(\frac{(1+z)\nu}{1.4 \text{ GHz}} \right)^{\alpha} \left(\frac{S_V}{\text{Jy}} \right). \quad (6)$$

This equation can be used to predict the SFR of a galaxy directly from observational radio data.

6 CONCLUSIONS

We have presented new 610-MHz GMRT observations of the ELAIS-N2 region, covering 6 deg^2 with 13 pointings. The typical noise level of each pointing is $\sim 90 \mu\text{Jy beam}^{-1}$ before primary beam correction. These radio observations have been combined with our previous surveys of the ELAIS-N1 and Lockman Hole regions, along with optical and infrared surveys, in order to create a sample of 510 galaxies in the three northern SWIRE fields, which have photometric redshifts and SFR estimates from Rowan-Robinson et al. (2008), infrared detections at 24 and $70 \mu\text{m}$, and radio detections at 610 MHz.

We have used the logarithmic ratio of infrared to radio flux densities, q'_{IR} , to discriminate between sources which are powered by star formation processes, and sources which may have a significant fraction of their radio emission resulting from AGN activity. By comparing the rest-frame 610-MHz radio luminosity to the Rowan-Robinson et al. (2008) SFR, we have identified a further set of sources which appear to be radio-quiet; we have demonstrated that these are likely to be galaxies where the template-fitting has been unsuccessful, leading to an over-estimation of the photometric redshifts and SFRs, although we discuss a number of real physical effects which could also be contributing to a reduction in the radio luminosity, such as the recent onset of starburst activity.

We have compared the Condon & Yin (1990) and Bell (2003) relationships between SFR and radio luminosity, and found that the Bell (2003) prescription is a better fit to our sample. By considering the ratio of radio luminosity and SFR, the ‘specific radio luminosity’, we have tested the validity of two of the assumptions that are commonly made when calculating the SFR history of the Universe from deep radio observations, namely that a relationship calibrated from local galaxies is applicable to galaxies at much higher redshift, and undergoing much greater starburst activity than seen in the local Universe. We find no redshift dependence for the specific radio luminosity, suggesting that there has been little change in the physical processes linking synchrotron radiation and star formation in star-forming galaxies over the redshift range $0 < z < 2$. No variation in the specific radio luminosity of galaxies with their SFR was found for a SFR in the range of 1 to $10^4 M_{\odot} \text{ yr}^{-1}$. This implies that the link between SFR and synchrotron luminosity is the same for massive starburst galaxies as it is for the more quiescent galaxies seen in the local Universe. We conclude that the Bell (2003) relationship between radio luminosity and SFR, calibrated from local galaxies, can successfully be applied to high-redshift, high-SFR galaxies, and present a generalised equation to link the

SFR of a galaxy to the observed flux density, redshift and radio spectral index.

ACKNOWLEDGEMENTS

TG thanks Dominic Ford for useful discussions, and the UK STFC for a Studentship. We thank the anonymous referee for helpful suggestions, and the staff of the GMRT who have made these observations possible. The GMRT is operated by the National Centre for Radio Astrophysics of the Tata Institute of Fundamental Research, India.

REFERENCES

- Ananthkrishnan S., 2005, in Sripathi Acharya B., Gupta S., Jagadeesan P., Jain A., Karthikeyan S., Morris S., Tonwar S., eds, Proc. 29th Int. Cosmic Ray Conf. Vol. 10, Tata Institute of Fundamental Research, Mumbai. pp 125–136
- Appleton P. N., et al., 2004, *ApJS*, 154, 147
- Baars J., Genzel R., Pauliny-Toth I., Witzel A., 1977, *A&A*, 61, 99
- Becker R. H., White R. L., Helfand D. J., 1995, *ApJ*, 450, 559
- Bell E. F., 2003, *ApJ*, 586, 794
- Bernet M. L., Miniati F., Lilly S. J., Kronberg P. P., Dessauges-Zavadsky M., 2008, *Nat*, 454, 302
- Beswick R. J., Muxlow T. W. B., Thrall H., Richards A. M. S., Garrington S. T., 2008, *MNRAS*, 385, 1143
- Bondi M., et al., 2007, *A&A*, 463, 519
- Boyle B. J., Cornwell T. J., Middelberg E., Norris R. P., Appleton P. N., Smail I., 2007, *MNRAS*, 376, 1182
- Capak P., et al., 2008, *ApJ*, 681, L53
- Carilli C. L., et al., 2008, *ApJ*, 689, 883
- Chi X., Wolfendale A. W., 1990, *MNRAS*, 245, 101
- Condon J. J., 1992, *ARA&A*, 30, 575
- Condon J. J., Anderson M. L., Helou G., 1991, *ApJ*, 376, 95
- Condon J. J., Cotton W. D., Broderick J. J., 2002, *AJ*, 124, 675
- Condon J. J., Cotton W. D., Yin Q. F., Perley R. A., Taylor G. B., Broderick G. B., 1998, *AJ*, 115, 1693
- Condon J. J., Yin Q. F., 1990, *ApJ*, 357, 97
- de Vaucouleurs G., de Vaucouleurs A., Corwin H. G., Buta R. J., Paturel G., Fouque P., 1991, *Third Reference Catalogue of Bright Galaxies. Vol. 1*, Springer-Verlag
- Douglas J. N., Bash F. N., Bozyan F. A., Torrence G. W., 1996, *AJ*, 111, 1945
- Draine B. T., 2003, *ARA&A*, 41, 241
- Dunkley J., et al., 2009, *ApJS*, 180, 306
- Fazio G., et al., 2004, *ApJS*, 154, 10
- Garn T., Alexander P., 2009, *MNRAS*, 394, 105
- Garn T., Green D. A., Hales S. E. G., Riley J. M., Alexander P., 2007, *MNRAS*, 376, 1251
- Garn T., Green D. A., Riley J. M., Alexander P., 2008a, *MNRAS*, 383, 75
- Garn T., Green D. A., Riley J. M., Alexander P., 2008b, *MNRAS*, 387, 1037
- Garrett M. A., 2002, *A&A*, 384, L19
- Haarsma D. B., Partridge R. B., Windhorst R. A., Richards E. A., 2000, *ApJ*, 544, 641
- Helou G., Bica M. D., 1993, *ApJ*, 415, 93
- Helou G., Soifer B. T., Rowan-Robinson M., 1985, *ApJ*, 298, L7
- Hopkins A. M., 2004, *ApJ*, 615, 209
- Hopkins A. M., Beacom J. F., 2006, *ApJ*, 651, 142
- Hopkins A. M., et al., 2003, *ApJ*, 599, 971
- Ibar E., et al., 2008, *MNRAS*, 386, 953
- Ibar E., Ivison R. J., Lal D. V., Best P. N., Green D. A., 2009, *MNRAS*, in press (astro-ph/0903.3600)
- Irwin M. J., Lewis J. R., 2001, *New Astron. Rev.*, 45, 105
- Kennicutt R. C., 1998, *ARA&A*, 36, 189
- Kronberg P. P., Bernet M. L., Miniati F., Lilly S. J., Short M. B., Higdon D. M., 2008, *ApJ*, 676, 70
- Léger A., Puget J. L., 1984, *A&A*, 137, L5
- Lilly S. J., Le Fevre O., Hammer F., Crampton D., 1996, *ApJ*, 460, L1
- Lonsdale C. J., Diamond P. J., Thrall H., Smith H. E., Lonsdale C. J., 2006, *ApJ*, 647, 185
- Lonsdale C. J., et al., 2003, *PASP*, 115, 897
- McMahon R. G., Walton N. A., Irwin M. J., Lewis J. R., Bunclark P. S., Jones D. H., 2001, *New Astron. Rev.*, 45, 97
- Madau P., Ferguson H. C., Dickinson M. E., Giavalisco M., Steidel C. C., Fruchter A., 1996, *MNRAS*, 283, 1388
- Magliocchetti M., Andreani P., Zwaan M. A., 2008, *MNRAS*, 383, 479
- Magnelli B., Elbaz D., Chary R. R., Dickinson M., Le Borgne D., Frayer D. T., Willmer C. N. A., 2009, *A&A*, 496, 57
- Mobasher B., Cram L., Georgakakis A., Hopkins A., 1999, *MNRAS*, 308, 45
- Murphy E. J., et al., 2006, *ApJ*, 638, 157
- Norris R. P., Middelberg E., Boyle B. J., 2007, in Afonso J., Ferguson H. C., Mobasher B., Norris R., eds, *Deepest Astronomical Surveys Vol. 380 of Astronomical Society of the Pacific Conference Series, ATLAS: Deep Radio Observations of Six Square Degrees*. pp 229–236
- Puget J. L., Léger A., 1989, *ARA&A*, 27, 161
- Richards A., et al., 2007, *A&A*, 472, 805
- Rieke G. H., Alonso-Herrero A., Weiner B. J., Pérez-González P. G., Blaylock M., Donley J. L., Marcillac D., 2009, *ApJ*, 692, 556
- Rieke G. H., et al., 2004, *ApJS*, 154, 25
- Rowan-Robinson M., 2003, *MNRAS*, 344, 13
- Rowan-Robinson M., et al., 2008, *MNRAS*, 386, 697
- Roy A. L., Norris R. P., Kesteven M. J., Troup E. R., Reynolds J. E., 1998, *MNRAS*, 301, 1019
- Sanders D. B., Mazzarella J. M., Kim D.-C., Surace J. A., Soifer B. T., 2003, *AJ*, 126, 1607
- Seymour N., et al., 2008, *MNRAS*, 386, 1695
- Smith H. E., Lonsdale C. J., Lonsdale C. J., Diamond P. J., 1998, *ApJ*, 493, L17
- Smolčić V., et al., 2009, *ApJ*, 690, 610
- Sopp H. M., Alexander P., 1991, *MNRAS*, 251, 14P
- Surace J. A., et al., 2005, *The SWIRE Data Release 2: Image Atlases and Source Catalogs for ELAIS-N1, ELAIS-N2, XMM-LSS and the Lockman Hole*, August 31, 2005 draft, available via http://swire.ipac.caltech.edu/swire/astromers/data_access.html
- Thompson T. A., Quataert E., Waxman E., Murray N., Martin C. L., 2006, *ApJ*, 645, 186
- Tresse L., et al., 2007, *A&A*, 472, 403
- Völk H. J., 1989, *A&A*, 218, 67
- Werner M., et al., 2004, *ApJS*, 154, 1
- Wilson C. D., Harris W. E., Longden R., Scoville N. Z., 2006, *ApJ*, 641, 763